THE JOURNAL OF PHYSICAL CHEMISTRY LETTERS
A JOURNAL OF THE AMERICAN CHEMICAL SOCIETY

Open Access
This article is licensed under CC-BY 4.0

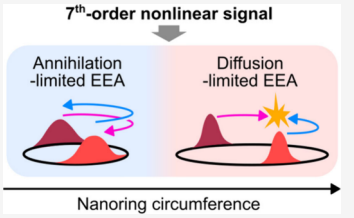
pubs.acs.org/JPCL
Letter

Single- and Multiexciton Dynamics in Porphyrin Nanorings

Erico M. Braun, Michael Jirasek, Harry L. Anderson, Stephen R. Meech, Ismael A. Heisler, and Giovanni Bressan*

Cite This: https://doi.org/10.1021/acs.jpclett.6c02850
Read Online
ACCESS | Metrics & More | Article Recommendations | Supporting Information

ABSTRACT: Exciton transport in molecular assemblies is typically studied in linear chains and polydisperse aggregates, where chain ends perturb the electronic structure and structural inhomogeneity can obscure size-dependent trends. Molecular nanorings overcome both limitations. They are end-group-free macrocycles with well-defined sizes, while their dimensions can be synthetically tuned from a few to several tens of porphyrin units. Here, we use intensity-cycled femtosecond transient absorption spectroscopy to disentangle single-exciton and multiexciton dynamics in a series of fully conjugated molecular nanorings containing 6−40 Zn-porphyrin units. By isolating the third-, fifth-, and seventh-order nonlinear responses, we independently track single-, two-, and three-exciton dynamics, respectively, enabling the ring-size dependence of exciton−exciton annihilation (EEA) to be determined without relying on *a priori* kinetic assumptions. The EEA rate decreases systematically with an increase in ring size, accompanied by a crossover from annihilation-limited to diffusion-limited EEA between 20 and 30 porphyrin units. The smallest nanoring exhibits no resolvable multiexciton dynamics, consistent with exciton delocalization across the entire ring or equivalent subinstrument response EEA, whereas larger rings exhibit increasingly diffusive exciton motion as static disorder limits delocalization. The retrieved exciton diffusion coefficients are 2−3 orders of magnitude higher than those we previously reported, indicating that the assumptions inherent to conventional intensity-dependent fitting can substantially underestimate exciton mobility.



Exciton−exciton annihilation (EEA) is a nonradiative process detrimental to the performance of organic photovoltaics,[1−6] yet beneficial to naturally occurring photosynthetic light-harvesting antennae, where it regulates function under a high degree of light exposure.[7−9] As a bimolecular process, its rate depends on exciton size and mobility.[10−12] Deliberately driving EEA at controlled excitation densities has therefore become a valuable spectroscopic handle for extracting exciton diffusion constants and delocalization lengths.[13−16]

The conventional route to quantifying EEA is to record the intensity dependence of femtosecond transient absorption (fsTA) data and fit the intensity-dependent component to a kinetic model, most commonly a random walk of the appropriate dimensionality with a time-dependent EEA rate.[13,15,17] We previously applied a ring-adapted version of this model to a series of butadiyne-linked Zn-porphyrin nanorings of general formula *c*-**P***n*, where ***n*** indicates the number of porphyrins (**P**) per ring (Figure 1a), extracting ring-size-dependent exciton diffusion coefficients.[18] However, the raw fsTA signals at the excitation densities needed to observe EEA contain nontrivial contributions in odd orders of nonlinear responses above $\chi^{(3)}$ arising from single- and multiparticle dynamics.[19−21] Disentangling such contributions typically requires *a priori* assumptions.

In 2023, Malý et al. showed that the different perturbative orders of the nonlinear optical response can be separated, isolating single- and multiexciton populations.[20] The method

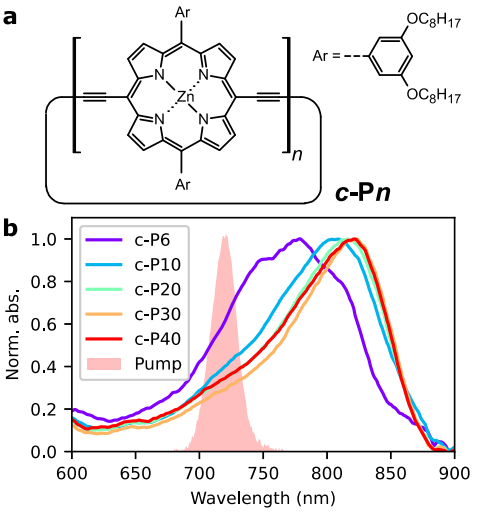


Figure 1. (a) Molecular structure of Zn-porphyrin nanorings *c*-**P***n* (top), where ***n*** (=6, 10, 20, 30, and 40) is the number of porphyrin units. (b) Normalized Q-band absorption spectra (solvent of toluene with 1% pyridine, concentration of <10 μM, path length of 1 mm) and 720 nm pump spectrum.

Received: August 25, 2026
Revised: November 2, 2026
Accepted: November 3, 2026

ACS Publications
© XXXX The Authors. Published by American Chemical Society

Downloaded from pubs.acs.org/jpclcd/article-pdf/doi/10.1021/acs.jpclett.6c02850/6911555l/acs.jpclett.6c02850.pdf by UNIV OF EAST ANGLIA user on 18 November 2026

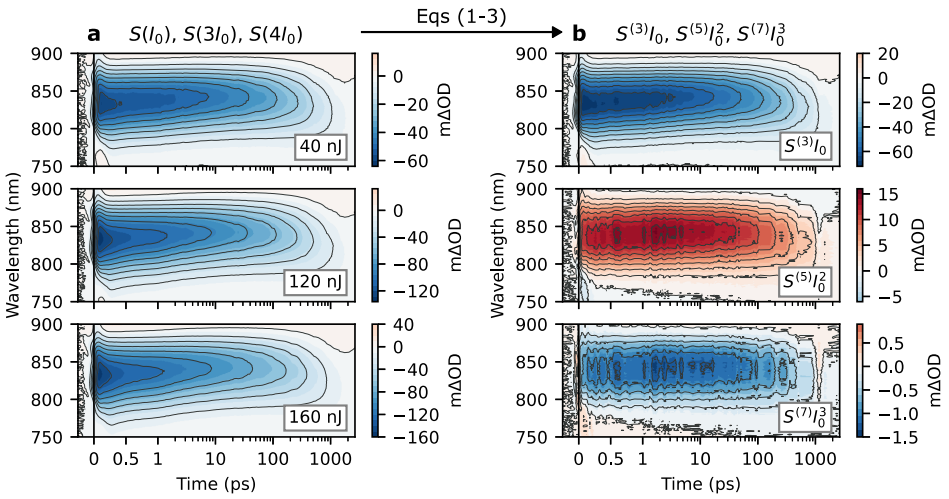


Figure 2. (a) *c*-**P20** fsTA color maps for 720 nm, 100 fs excitation pulses at the three intensities used (40, 120, and 160 nJ) for the nonlinear order extraction scheme. (b) Extracted nonlinear orders $S^{(n)}$ of *c*-**P20** using eqs 1−3. Note that the time axis is linear up to 1 ps and logarithmic after.

relies on "intensity cycling", conceptually similar to the phase-cycling strategies commonly employed to isolate the desired signal from background contributions in (partially or fully) collinear implementations of two-dimensional spectroscopies.[20−22] Porphyrin nanorings are a natural test bed for this capability. Such systems combine strongly coupled, delocalized, red to near-infrared Q-band excitations with topology imposing well-defined periodic boundary conditions on exciton mobility,[18,23−25] in stark contrast with the linear chains typically used to describe EEA in conjugated polymers and aggregates. The wide size tunability of *c*-**P*n*** nanorings, achieved from a single chromophore and (conjugated) linkage motif, makes them a rare system in which exciton transport regimes can be systematically investigated in the absence of end groups, perturbing the electronic structure and conformation.

Here, we apply the method of Malý et al.[20] to a nanoring series (*c*-**P6**−*c*-**P40**), extracting one-, two-, and three-exciton dynamics separately and determining EEA rates and annihilation regimes as a function of ***n***. We demonstrate a size-dependent crossover from annihilation- to diffusion-limited EEA that could not be resolved with our previous analysis, providing new insight into how delocalization and topology jointly modulate exciton transport in cyclic conjugated supramolecular chromophore assemblies.

The general structure and Q-band absorption spectra of the Zn-porphyrin nanorings (*c*-**P*n***) are shown in Figure 1. The absorption peak undergoes a red-shift and a loss of structure with an increase in ring size, consistent with an exciton more delocalized around the ring,[23,24,26] until it saturates between 20 and 30 porphyrin units. Both saturation and loss of structure are consequences of static disorder, which limits the exciton size and makes the electronic properties of larger nanorings approach those of linear porphyrin oligomers.[26]

Intensity-cycled fsTA with 100 fs, 720 nm excitation pulses (spectrum shown in Figure 1) was applied to investigate multiexciton dynamics in these samples arising from Q-band photoexcitation. The intensity cycling followed the $I_r = \{I_0, 3I_0, 4I_0\}$ cycling scheme of Malý et al.[20] using a base pump energy per pulse (I_0) of 40−50 nJ depending on the sample absorbance at 720 nm. Third- to seventh-order nonlinear signals $S^{(n)}$ were extracted by combining the measured signals at each intensity $S(I_r)$ using the following set of equations:[20,21]

$$S^{(3)}(I_0) = 2S(I_0) - \frac{2}{3}S(3I_0) + \frac{1}{4}S(4I_0) \quad (1)$$

$$S^{(5)}(I_0) = -\frac{7}{6}S(I_0) + \frac{5}{6}S(3I_0) - \frac{1}{3}S(4I_0) \quad (2)$$

$$S^{(7)}(I_0) = \frac{1}{6}S(I_0) - \frac{1}{6}S(3I_0) + \frac{1}{12}S(4I_0) \quad (3)$$

Following eqs 1−3, the extracted third-order signal $S^{(3)}$ is only proportional to processes that scale linearly with intensity (i.e., $\chi^{(3)}$), making it report directly on the single-exciton population without contamination from higher-order processes. The higher orders, $S^{(5)}$ and $S^{(7)}$, are proportional to processes that scale with I_0^2 and I_0^3, respectively ($\chi^{(5)}$ and $\chi^{(7)}$), and therefore, they may contain contributions from two- and three-exciton processes, respectively. Thus, this method allows for the analysis of the uncontaminated single-exciton dynamics at higher intensities, where the signal-to-noise ratio (SNR) is higher, and to the analysis of the dynamics of a number of excitons up to the number of orders extracted.

The quality of the nonlinear order isolation procedure was checked by comparing the extracted third-order signal $S^{(3)}$ against a scaled low-power reference measurement[20,27] of ∼10 μW (i.e. 10 nJ/pulse), which creates on average 0.02−0.16 exciton per nanoring (Table S1) depending on the sample and thus contains negligible multiexciton signals. We report the comparison between the extracted third-order signal and the low-power reference for each sample in Figures S1 and S2, showing excellent agreement between the two. In addition, we further checked the possibility of higher-order contaminations (ninth and above) in the data sets by fitting saturation curves of the transient signal at T = 100 fs, corresponding to the signal maximum, as a function of intensity (Figure S3). Even at the highest intensities used, higher-order contaminations represent less than 2% of the total signal, further validating the extraction procedure with the chosen intensities.

As a representative example for nonlinear order extraction, Figure 2a presents the fsTA maps in the 750−900 nm range of *c*-**P20**, corresponding to the ground state bleach (GSB) and stimulated emission (SE), while isolated nonlinear signals for

Downloaded from pubs.acs.org/jpclcd/article-pdf/doi/10.1021/acs.jpclett.6c02850/6911555l/acs.jpclett.6c02850.pdf by UNIV OF EAST ANGLIA user on 18 November 2026

https://doi.org/10.1021/acs.jpclett.6c02850
J. Phys. Chem. Lett. XXXX, XXX, XXX−XXX

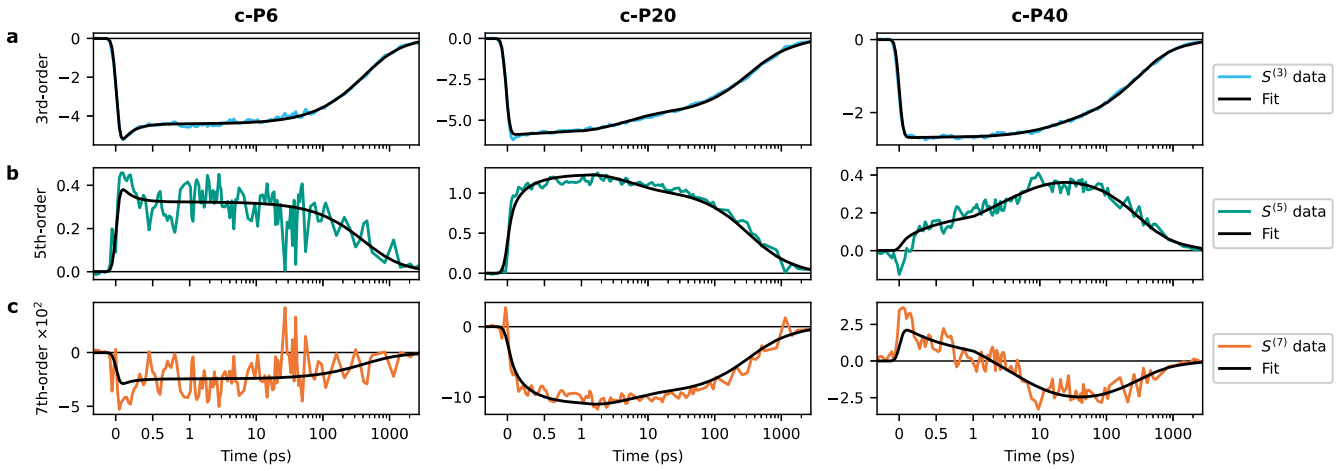


Figure 3. GSB+SE band-integrated $S^{(n)}$ traces for samples *c*-**P6**, *c*-**P20**, and *c*-**P40** (columns). (a) Third-order traces, fitted to a sum of three exponential decays in all three samples. (b) Fifth-order traces, fitted to a rescaled third-order fit in *c*-**P6** and to eq 4 for *c*-**P20** and *c*-**P40**. (c) Seventh-order traces, with *c*-**P6**'s also fitted to a rescaled third-order fit while *c*-**P20** and *c*-**P40** traces were fitted to eq 5. For all higher-order fits, the parameters corresponding to $S^{(3)}$ in eqs 4 and 5 were kept fixed. Fitted parameters are summarized in Table 1.

Table 1. Fitted Third-Order Time Constants and Amplitudes Using Three Parallel Exponential Decays for $S^{(3)}$, Fitted EEA Rate Constants, and *f* Parameters Using eqs 4 and 5 with the Diffusion-Limited Effective Model (eq 6) and Calculated Diffusion Constants *D* and Diffusion Lengths $L_D = \sqrt{D\langle\tau\rangle}$, Where $\langle\tau\rangle$ Is the Average Lifetime.

	third-order		fifth-order			seventh-order
sample	τ_i (ps)	A_i (±0.1 mOD)	k_{EEA} ($ps^{-0.5}$)	D (cm^2/s)	L_D (nm)	f
c-**P6**	0.15 ± 0.02, 360 ± 20, 1480[a]	−1.6, −3.2, −1.2	n/a[b]	n/a[b]	n/a[b]	n/a[b]
c-**P10**	0.4 ± 0.1, 650 ± 50, 930[a]	−0.1, −2.8, −0.1	3.0 ± 0.5[c]	8 ± 3[c]	700 ± 200[c]	2[d]
c-**P20**	4.9 ± 0.3, 290 ± 20, 1240[a]	−1.2, −3.3, −1.4	1.55 ± 0.06	5.8 ± 0.4[e]	530 ± 30[e]	2.8 ± 0.2
c-**P30**	10 ± 2, 420 ± 10, 1180[a]	−0.4, −5.0, −0.8	0.52 ± 0.02	1.47 ± 0.08	280 ± 10	3.9 ± 0.3
c-**P40**	20 ± 2, 290 ± 20, 1240[a]	−0.4, −1.8, −0.5	0.24 ± 0.02	0.57 ± 0.06	158 ± 8	20 ± 10

[a]Longest time constants were fixed to the same value retrieved in global analysis. [b]*c*-**P6** higher-order traces were fitted to a rescaled $S^{(3)}_{fit}$. [c]IRF-limited. [d]Fixed at the value of no three-exciton contribution in $S^{(7)}$ ($f = 2$). [e]Underestimated due to annihilation-limited EEA.

all samples can be found in Figures S4−S8. The GSB+SE region was chosen due to its high SNR, facilitating the observation of higher-order contributions. fsTA data sets were acquired at 40, 120, and 160 nJ/pulse. Figure 2b shows the third- to seventh-order signals for *c*-**P20**, isolated by applying eqs 1−3 to the data sets in Figure 2a. Focusing first on the single-exciton dynamics, we analyzed extracted third-order signals $S^{(3)}$ using global analysis as implemented in pyglotaran.[28] A sequential decay model of three compartments was used for *c*-**P6** and *c*-**P10** and of four compartments for *c*-**P20**−*c*-**P40**, yielding the evolution-associated difference spectra (EADS) shown in Figures S9 and S10 and discussed in more detail in the Supporting Information. Overall, retrieved EADS and time constants of the third-order signals are in good agreement with the literature.[18,23,24,29]

As nanorings larger than *c*-**P10** present a red-shift of the third-order negative signal over the first picosecond, we spectrally integrated the isolated nonlinear signals in the GSB +SE range (700−850 nm for *c*-**P6** and 750−900 nm for *c*-**P10**−*c*-**P40**) to remove this spectral evolution and simplify the analysis of the higher nonlinear orders (Figures S4−S8). The resulting third- to seventh-order band-integrated traces, reporting directly on the excitonic populations and oscillator strengths,[30] are presented in Figure 3 for samples *c*-**P6**, *c*-**P20**, and *c*-**P40** (GSB+SE band-integrated traces for *c*-**P10** and *c*-**P30** can be found in Figures S11 and S12, respectively). The integrated third-order response can be well fitted to a sum of three exponential decays ($S^{(3)}_{fit}(t) = \sum_{i=1}^{3} A_i e^{-t/\tau_i}$) convolved with a 100 fs fwhm Gaussian instrument response function (IRF), yielding the time constants listed in Table 1. These are in good agreement with the three longer components fitted through global analysis (Figures S9 and S10). The fifth- and seventh-order extracted signals display alternating signs relative to the third-order signals, with the exception of *c*-**P40**'s seventh-order signal, which changes sign during the pump−probe delay time, a behavior that will be addressed shortly.

The alternating sign in the isolated nonlinear signals stems from each term $P^{(N)}$ in the nonlinear polarization expansion possessing a $(-i)^N$ prefactor,[19] which alternates the sign between consecutive odd-*N* terms.[22,31] However, the observation of higher-order signals does not necessarily indicate multiexciton dynamics, as saturation of the electronic transition is also a process that contributes to the higher-order responses of two-level systems.[20] Nevertheless, these saturation signals follow the same kinetic profile of the single-exciton population, i.e., the third-order response, and can thus be identified by comparing the isolated higher-order signals with the third-order one.[31,32]

Extracted fifth-order signals (Figure 3b) exhibit ring-size-dependent kinetics at early times. The fifth-order trace of *c*-**P6** follows the kinetic profile of the (inverted) third-order response, while in *c*-**P20**, a rise time is observed. This rise time becomes slower with the increase in nanoring size, as shown in *c*-**P30** (Figure S12b) and *c*-**P40** (Figure 3b). The

https://doi.org/10.1021/acs.jpclett.6c02850
J. Phys. Chem. Lett. XXXX, XXX, XXX−XXX

Downloaded from pubs.acs.org/jpclcd/article-pdf/doi/10.1021/acs.jpclett.6c02850/6911555l/acs.jpclett.6c02850.pdf by UNIV OF EAST ANGLIA user on 18 November 2026

seventh-order signals (Figure 3c) broadly follow a similar trend. The seventh-order response of *c*-**P6** is a weaker "replica" of the third-order signal. A rise time, slower than that contributing to the fifth-order signal, is observed in *c*-**P20** and *c*-**P30** (Figure S12c), while a sign inversion ∼3 ps after photoexcitation is observed for *c*-**P40**. These dynamics in the fifth- and seventh-order responses report directly on EEA, which was previously reported in nanorings with more than 10 porphyrins.[18]

To extract EEA time scales, the fifth- and seventh-order traces were fitted to equations describing the nonlinear responses derived by Malý et al.,[20] which assume the pump pulse can create up to m identical excitations in each molecule. In the case in which EEA is much faster than relaxation to the ground state—which is the case for the nanorings, where EEA happens within the first tens of picoseconds (Figure 3) while the excited state lifetime is ∼500 ps[23,24,26]—conversion of the populations of each n-exciton manifold is only due to EEA, described by intermanifold (effective) annihilation rates $k_{n\to n-1}(t)$ (eq S2, with more details given in section 6 of the Supporting Information). Assuming only pairwise EEA, the two- and three-exciton annihilation rates can be written as $k_{2\to 1}(t) = k_A(t)$ and $k_{3\to 2}(t) = fk_A(t)$,[15,17,27] respectively, where $k_A(t)$ is the effective (pairwise) annihilation rate and $f \geq 3$ is a rate-enhancement factor in the three-exciton manifold[20,27] (see below). The expressions for the nonlinear responses are found by summing all of the relevant double-sided Feynman diagrams for each nonlinear order while taking into account the population of each n-exciton manifold, and in principle, the resulting $S^{(5,7)}(t)$ expressions depend on the number of excitations m.[20] Their dependence with m, however, is quickly saturated when $m > 6$,[20] and since we can assume each porphyrin brings one new state to the singly excited state manifold of the nanoring, we take m as the total number of porphyrin units composing each ring and apply the large m limit of the expressions, which results in

$$S_{\text{fit}}^{(5)}(t) = A_5\left[1 - \exp\left(-\int k_A(t)\,\mathrm{d}t\right)\right] \times S_{\text{fit}}^{(3)}(t) \tag{4}$$

$$S_{\text{fit}}^{(7)}(t) = A_7\left[1 - \frac{2f-3}{f-1}\exp\left(-\int k_A(t)\,\mathrm{d}t\right) + \frac{f-2}{f-1} \times \exp\left(-f\int k_A(t)\,\mathrm{d}t\right)\right] \times S_{\text{fit}}^{(3)}(t) \tag{5}$$

where A_5 and A_7 are proportionality amplitudes and $S_{\text{fit}}^{(3)}(t)$ is the fitted third-order response in each sample, describing losses of the oscillator strength and the long-time behavior of all nonlinear orders. Equations 4 and 5 were also convolved with a 100 fs Gaussian IRF for the fitting procedure.

The functional form of the EEA rate in eqs 4 and 5 depends on the dimensionality of exciton diffusion.[15,27] For the low concentrations used (approximately micromolar) and investigated time scales, intermolecular energy transfer is negligible, and exciton diffusion is thus confined to each nanoring. Treating EEA as a one-dimensional diffusion-limited reaction, we applied the Noyes-Smoluchowski relation[15,17,27]

$$k_A(t) = k_{\text{EEA}}t^{-1/2} = \frac{1}{L}\sqrt{\frac{8D}{\pi t}} \tag{6}$$

where $k_{\text{EEA}} = \sqrt{8D/\pi L^2}$ is the effective EEA rate constant (in $\text{ps}^{-0.5}$), L is the available diffusion size, and D is the diffusion constant. This expression is valid for excitons undergoing normal diffusion in large available diffusion sizes L and because of this can overestimate the diffusion for time scales longer than the exciton revolution time ($\Delta T_{\text{rev}} = L^2/2D$) around the finite L nanoring.[17] Despite these deficiencies, we use eq 6 as an effective model to better compare with previous results where the same rate expression was used.[15,18,27,33] While fitting $S^{(5)}$ using eqs 4 and 6, the parameters of $S_{\text{fit}}^{(3)}(t)$ (amplitudes and time constants) were held fixed, leaving only proportionality amplitude A_5 and effective EEA rate constant k_{EEA} (in $\text{ps}^{-0.5}$) as free parameters. Similarly, parameters from $S_{\text{fit}}^{(3)}(t)$ and k_{EEA} were also held fixed during $S^{(7)}$ fitting, reducing the number of free parameters and making the optimized values more robust to the initial guesses.

At each nonvanishing nonlinear order higher than the third, a higher n-exciton manifold process contributes to the signal.[20,34] This is demonstrated in both eqs 4 and 5, where the second term describes decay from the two-exciton manifold, while the third term in eq 5 describes decay from the three-exciton one. The kinetics of the latter introduces parameter f into eq 5, which informs on the EEA regime. For annihilation-limited EEA, where the EEA-limiting step is an annihilation probability of less than one (i.e., two excitons may encounter without necessarily being annihilated), $f = \binom{3}{2} = 3$ because there are three different ways for three independent excitons to annihilate pairwise. For diffusion-limited EEA, where the exciton encounter rate is limited by diffusion, f is usually greater than 3 due to diffusion accelerating EEA in the three-exciton manifold through three-exciton encounters.[20,27] These encounters lead to a greater loss of excitonic population when compared to the annihilation-limited case, which is manifested through $S^{(7)}$ (eq 5) becoming positive at early times for $f > 3$ (more GSB+SE signal is lost due to three-exciton encounters) followed by a sign inversion, while for $f = 3$ (annihilation-limited) $S^{(7)}$ is negative for all times greater than zero (the dependence of eq 5 with f is shown in Figure S13). Each of the previous behaviors is exemplified in the seventh-order traces of *c*-**P40** and *c*-**P20** (Figure 3c), indicating that EEA is diffusion-limited in *c*-**P40** while annihilation-limited in *c*-**P20**.

Fitted parameters are summarized in Table 1. The recovered EEA rate constants follow a decreasing trend as the nanoring size increases, starting at 3.0 $\text{ps}^{-0.5}$ in *c*-**P10** (Figure S11), likely limited by the ∼100 fs IRF, and decreasing to 0.24 $\text{ps}^{-0.5}$ in *c*-**P40**. Alongside the decrease in the EEA rate constant, the annihilation regime also changes as the nanoring increases in size. It starts annihilation-limited in *c*-**P20** ($f = 3$ within the uncertainty) and becomes diffusion-limited in *c*-**P30** (Figure S12) and *c*-**P40** ($f > 3$). To the best of our knowledge, such a trend between the measured EEA regime and molecular size has not been reported previously. For the two smallest nanorings, no contributions from three-exciton processes are observed in *c*-**P10**'s seventh-order signal, nor in two-exciton processes in *c*-**P6**'s fifth-order signal. To account for these two cases, *c*-**P10**'s seventh-order signal was fitted by eq 5 with a fixed f value of 2, which is an equivalent way of removing the three-exciton contribution from the fit (third term in eq 5); on the other hand, *c*-**P6**'s fifth- and seventh-order traces were fitted to rescaled versions of the third-order fit, $S_{\text{fit}}^{(5,7)}(t) =$

https://doi.org/10.1021/acs.jpclett.6c02850
J. Phys. Chem. Lett. XXXX, XXX, XXX−XXX

Downloaded from pubs.acs.org/jpclcd/article-pdf/doi/10.1021/acs.jpclett.6c02850/6911555l/acs.jpclett.6c02850.pdf by UNIV OF EAST ANGLIA user on 18 November 2026

$A_{5,7}S^{(3)}_{fit}(t)$, with both respective approaches producing good fits (Figure S11 and Figure 3, respectively). This last result indicates *c*-**P6** behaves effectively like a two-level system, where nonlinear orders above $\chi^{(3)}$ show only saturation of the electronic transition with no detectable evidence of multi-exciton contributions with this time resolution.[20]

For nanorings with resolvable EEA dynamics, diffusion constants D (in square centimeters per second) can be calculated from fitted rate constants k_{EEA} and available diffusion size L in each nanoring using eq 6. To calculate L, we assumed the rings to be perfectly circular, with L being equal to their circumference. For each ring *c*-**P*n***, circumferences were extrapolated from the *c*-**P6** value of $L_{c\text{-}P6}$ = 7.5 nm, itself calculated from the 2.4 nm diameter measured by SAXS,[25] by assuming the circumferences to be directly proportional to the number of porphyrins in each ring (details in section 7 of the Supporting Information). Diffusion constants are then calculated as $D = \pi L_{c\text{-}Pn}{}^2 k_{EEA}{}^2/8$, and their values are listed in Table 1. D values follow the same trend as the EEA rate constant, showing that the exciton diffuses more slowly as the nanoring circumference increases. Also calculated are diffusion lengths $L_D = \sqrt{D\langle\tau\rangle}$, where $\langle\tau\rangle$ is the amplitude-averaged lifetime, which all exceed the circumference values by at least 3 times (a comparison between diffusion lengths and nanoring circumference is shown in Table S2). In *c*-**P20**, where EEA is annihilation-limited, the recovered diffusion constant and length are underestimated due to suppression of the annihilation rate by the annihilation probability of <1, while in *c*-**P10**, they are likely IRF-limited. We also note the values reported here are 2−3 orders of magnitude greater than the previous diffusion constants reported for *c*-**P10**−*c*-**P40**.[18] We attribute this discrepancy to the nonlinear order extraction giving direct access to the n-exciton populations, allowing a more accurate determination of the annihilation rate by avoiding the previously used model that assumed a bulk description of EEA[35] (many excitons per nanoring), a condition that is not satisfied even at the highest intensities used, where on average two to three excitons are created per nanoring. Finally, using the diffusion constants calculated here, we can also estimate the time an exciton takes to perform a full revolution around the ring as $\Delta T_{rev} = L^2/2D$, giving approximate values of 100 fs for *c*-**P10**, 0.5 ps for *c*-**P20**, 5 ps for *c*-**P30**, and 22 ps for *c*-**P40**. These exciton revolution times are on time scales similar to those of the fastest EADS components and better approach the simulated values for population transfer around similar nanorings,[36] indicating that significant exciton motion modulates the (single exciton) third-order response.

Theoretical and experimental studies show that EEA rates depend on the exciton's effective delocalization length.[37−41] Porphyrin nanorings can be considered J-aggregates[36,42] with periodic boundary conditions to exciton motion imposed by their topology and display extensive excitonic delocalization following photoexcitation.[23,26,43] In such systems, measured EEA rates reflect the relative exciton delocalization length against the size of the nanoring, and also how fast excitons can diffuse around it. In *c*-**P20**, EEA proceeds on time scales comparable to the 100 fs IRF and in the annihilation-limited regime, meaning that excitons meet each other, possibly multiple times, on such a time scale without being annihilated. This is likely also the case for the smallest nanorings, *c*-**P6** and *c*-**P10**, where, despite no direct observation of the EEA regime through three-exciton processes, previous anisotropy studies have estimated initial delocalization lengths following photoexcitation to be comparable to the total number of porphyrins,[23,26] which would further facilitate pairwise exciton encounters in the confined geometry of the nanorings. In the case of *c*-**P6**, where delocalization appears to extend over the entire ring,[26] EEA (if present) must happen on time scales shorter than the ∼100 fs IRF, as evidenced by the lack of resolvable multiexciton contributions in the fifth- and seventh-order traces (Figure 3 for *c*-**P6**). As the number of porphyrins in the ring (i.e., its circumference) increases, EEA becomes slower and enters the diffusion-limited regime at a size between 20 and 30 porphyrin units. This directly correlates to the previously reported exciton delocalization lengths becoming smaller relative to the ring size in *c*-**P30** and *c*-**P40**,[26] which is manifested by the saturation of the red-shift in their absorption spectra and their response resembling progressively more their linear counterparts as size increases.[26] Such exciton localization effects can be attributed to disorder becoming more pronounced with ring size, which modifies the excited state energetic landscape and leads to limited initial delocalization lengths (estimated at 10−20 porphyrins[23,24,26]) and slower excitonic diffusion.

The results obtained here clarify the parameters governing EEA in other tetrapyrrole-based systems such as photosynthetic light-harvesting complexes, where even at very low fluences non-negligible EEA decay channels are observed.[9,12,44] Recently, Zhang et al. analyzed EEA kinetics in a photosystem II supercomplex using the same nonlinear order extraction procedure, reporting subdiffusive EEA with time-dependent rate $k_A(t) \propto t^{-0.49}$,[45] practically identical to the time dependence of the diffusion rate used in this work. In their case, however, the fractional exponent was interpreted as arising from exciton subdiffusion in the three-dimensional supercomplex rather than one-dimensional (effective) normal diffusion. The fact that two different dimensionalities can lead to similar effective annihilation rates is a call for attention, with careful analysis being required in the interpretation of exciton diffusion in nonlinear order-separated fsTA. Furthermore, the diffusion coefficients retrieved for diffusion-limited nanorings *c*-**P30** and *c*-**P40** ($D \approx$ 1.5 to 0.6 cm^2/s) are 10−100 times greater than the intraring exciton mobility of the B850 ring of LH2. Approximating exciton diffusion in B850 as a nearest-neighbor random walk, reported hopping time τ_h of 0.27 ps[46] across the 0.9 nm bacteriochlorophyll spacing (a) corresponds to an effective one-dimensional diffusion coefficient $D = a^2/2\tau_h$ of 10^{-2} cm^2/s. This difference can be directly attributed to structural differences between the two systems. B850 is a considerably smaller ring (18 bacteriochlorophylls). Its exciton is delocalized over only approximately three pigments,[46] and its chromophores are coupled through space. On the contrary, the nanorings are fully conjugated and support delocalization over more than 10 porphyrin units.[24,26]

METHODS

c-**P*n*** samples were dissolved in toluene with 1% pyridine to avoid aggregation and prepared in static 1 mm path length cuvettes with an OD of 0.3 at the absorption maximum, corresponding to concentrations of <10 μM. Femtosecond transient absorption (fsTA) spectroscopy was carried out using a previously described fsTA/half-broadband 2DES spectrometer.[47,48] Briefly, a regenerative amplified Ti:sapphire laser (Spitfire Ace, Spectra-Physics) producing 120 fs pulses at 800

Downloaded from pubs.acs.org/jpclcd/article-pdf/doi/10.1021/acs.jpclett.6c02850/6911555l/acs.jpclett.6c02850.pdf by UNIV OF EAST ANGLIA user on 18 November 2026

https://doi.org/10.1021/acs.jpclett.6c02850
J. Phys. Chem. Lett. XXXX, XXX, XXX−XXX

nm and a 1 kHz repetition rate was used to pump two commercial optical parametric amplifiers (OPA, TOPAS Prime, Spectra-Physics). Pump pulses were derived from one OPA that outputs 100 fs, 720 nm pulses, with the intensity finely adjusted by a variable neutral-density (ND) filter wheel and recorded with an optical power meter (Ophir 7Z01550 Nova II) before each measurement. The IRF width of ∼100 fs was determined by measuring the instantaneous nonresonant response induced by the pump pulse in neat toluene (Figure S14). The pump energy per pulse was varied in the range of 40−200 nJ to perform intensity cycling (details in the text), while the low-power reference measurements were set to ∼10 nJ. Pump energies were found to be stable within the 1 μW resolution of the power meter, corresponding to <1 nJ fluctuations in the energy-per-pulse values. The 550−1200 nm probe pulses were created by focusing the attenuated 1250 nm output of the second OPA in a 3 mm thick sapphire plate. A half-wave plate and polarizer pair in each arm ensured the relative pump and probe polarizations were set at the magic angle (∼54.7°), with subsequent metallic spherical mirrors focusing the pump and probe to spot sizes of 160 and 80 μm, respectively, at the sample position. Relative delay T between pump and probe pulses was introduced by mechanically delaying the pump with a retroreflector mounted on a linear translation stage (Physik Instrumente), yielding T values from −0.5 to 2500 ps. Probe pulses were recollimated after the sample and were detected on a shot-to-shot basis using a prism-based custom-built spectrometer and a linear CCD camera (Stresing). For each sample, fsTA was performed under identical conditions except for the varying pump pulse intensity. The recorded data sets were postprocessed for background subtraction and chirp correction (identical time-zero parameters for all intensities were used) and then combined to yield the extracted $S^{(n)}$ signals by a Python script using the NumPy[49] package. Fitting of the nonlinear orders was performed with the SciPy[50] curve fitting tool by first fitting $S^{(3)}$, then $S^{(5)}$ with only k_{EEA} and A_5 as free parameters, and, finally, $S^{(7)}$ with only f and A_7 as free parameters. Uncertainties in the calculated parameters were obtained by uncertainty propagation from the fit uncertainties (see section 7 of the Supporting Information).

■ ASSOCIATED CONTENT

Supporting Information

The Supporting Information is available free of charge at https://pubs.acs.org/doi/10.1021/acs.jpclett.6c02850.

Average number of excitons per nanoring at low pump power, comparison between $S^{(3)}$ and low-power reference and saturation curves and fits, global analysis of third-order data, isolated and band-integrated third- to seventh-order signals for all samples, $S^{(5)}$ and $S^{(7)}$ nonlinear model description, and procedure for the estimation of diffusion constants and nanoring circumference and nonresonant response in neat toluene (PDF)

■ AUTHOR INFORMATION

Corresponding Author

Giovanni Bressan − *School of Chemistry, Pharmacy & Pharmacology, University of East Anglia, Norwich NR4 7TJ, United Kingdom;* orcid.org/0000-0001-7801-8495; Email: G.Bressan@uea.ac.uk

Authors

Erico M. Braun − *Departamento de Física, Universidade Federal do Rio Grande do Sul (UFRGS), 9500 Porto Alegre, Brazil; School of Chemistry, Pharmacy & Pharmacology, University of East Anglia, Norwich NR4 7TJ, United Kingdom;* orcid.org/0009-0003-5022-7502

Michael Jirasek − *Chemistry Research Laboratory, Department of Chemistry, University of Oxford, Oxford OX1 3TA, United Kingdom*

Harry L. Anderson − *Chemistry Research Laboratory, Department of Chemistry, University of Oxford, Oxford OX1 3TA, United Kingdom;* orcid.org/0000-0002-1801-8132

Stephen R. Meech − *School of Chemistry, Pharmacy & Pharmacology, University of East Anglia, Norwich NR4 7TJ, United Kingdom;* orcid.org/0000-0001-5561-2782

Ismael A. Heisler − *Departamento de Física, Universidade Federal do Rio Grande do Sul (UFRGS), 9500 Porto Alegre, Brazil;* orcid.org/0000-0002-8581-4745

Complete contact information is available at: https://pubs.acs.org/10.1021/acs.jpclett.6c02850

Notes

The authors declare no competing financial interest.

■ ACKNOWLEDGMENTS

E.M.B. thanks the Brazilian agency CNPq for his studentships (141128/2022-4 and SWE200581/2025-2). S.R.M. is grateful to EPSRC for financial support (EP/V00817X/1 and EP/J009148/1). I.A.H. is grateful to CNPq for financial support (403208/2024-6). G.B. is grateful to the Leverhulme Trust for funding him through an Early Career Fellowship (Grant ECF-2023-195).

■ REFERENCES

(1) Hader, K.; May, V.; Lambert, C.; Engel, V. Identification of Effective Exciton−Exciton Annihilation in Squaraine−Squaraine Copolymers. *Phys. Chem. Chem. Phys.* **2016**, *18* (19), 13368−13374.

(2) Kepler, R. G.; Valencia, V. S.; Jacobs, S. J.; McNamara, J. J. Exciton-Exciton Annihilation in Poly (*p*-Phenylenevinylene) Films. *Synth. Met.* **1996**, *78* (3), 227−230.

(3) Fairbairn, N. J.; Vodianova, O.; Schmidt, B. V. K. J.; Hedley, G. J. Highly Efficient Exciton-Exciton Annihilation in Single Conjugated Polymer Chains. *Nat. Commun.* **2026**, *17* (1), 731.

(4) Nguyen, T.-Q.; Martini, I. B.; Liu, J.; Schwartz, B. J. Controlling Interchain Interactions in Conjugated Polymers: The Effects of Chain Morphology on Exciton−Exciton Annihilation and Aggregation in MEH−PPV Films. *J. Phys. Chem. B* **2000**, *104* (2), 237−255.

(5) Akselrod, G. M.; Tischler, Y. R.; Young, E. R.; Nocera, D. G.; Bulovic, V. Exciton-Exciton Annihilation in Organic Polariton Microcavities. *Phys. Rev. B* **2010**, *82* (11), 113106.

(6) Wang, K.; Chen, H.; Zhang, J.; Zou, Y.; Yang, Y. Intrachain and Interchain Exciton−Exciton Annihilation in Donor−Acceptor Copolymers. *J. Phys. Chem. Lett.* **2021**, *12* (16), 3928−3933.

(7) van Grondelle, R. Excitation Energy Transfer, Trapping and Annihilation in Photosynthetic Systems. *Biochim. Biophys. Acta BBA - Rev. Bioenerg.* **1985**, *811* (2), 147−195.

(8) Ma, F.; Yu, L.-J.; Hendrikx, R.; Wang-Otomo, Z.-Y.; van Grondelle, R. Excitonic and Vibrational Coherence in the Excitation Relaxation Process of Two LH1 Complexes as Revealed by Two-Dimensional Electronic Spectroscopy. *J. Phys. Chem. Lett.* **2017**, *8* (12), 2751−2756.

(9) Rutkauskas, D.; Chmeliov, J.; Johnson, M.; Ruban, A.; Valkunas, L. Exciton Annihilation as a Probe of the Light-Harvesting Antenna Transition into the Photoprotective Mode. *Chem. Phys.* **2012**, *404*, 123−128.

Downloaded from pubs.acs.org/jpclcd/article-pdf/doi/10.1021/acs.jpclett.6c02850/6911555l/acs.jpclett.6c02850.pdf by UNIV OF EAST ANGLIA user on 18 November 2026

(10) May, V. Kinetic Theory of Exciton−Exciton Annihilation. *J. Chem. Phys.* **2014**, *140* (5), 054103.
(11) Renger, T.; May, V. Theory of Multiple Exciton Effects in the Photosynthetic Antenna Complex LHC-II. *J. Phys. Chem. B* **1997**, *101* (37), 7232−7240.
(12) Valkunas, L.; Trinkunas, G.; Liuolia, V.; Van Grondelle, R. Nonlinear Annihilation of Excitations in Photosynthetic Systems. *Biophys. J.* **1995**, *69* (3), 1117−1129.
(13) Shaw, P. E.; Ruseckas, A.; Peet, J.; Bazan, G. C.; Samuel, I. D. W. Exciton−Exciton Annihilation in Mixed-Phase Polyfluorene Films. *Adv. Funct. Mater.* **2010**, *20* (1), 155−161.
(14) Lewis, A. J.; Ruseckas, A.; Gaudin, O. P. M.; Webster, G. R.; Burn, P. L.; Samuel, I. D. W. Singlet Exciton Diffusion in MEH-PPV Films Studied by Exciton−Exciton Annihilation. *Org. Electron.* **2006**, *7* (6), 452−456.
(15) Engel, E.; Leo, K.; Hoffmann, M. Ultrafast Relaxation and Exciton−Exciton Annihilation in PTCDA Thin Films at High Excitation Densities. *Chem. Phys.* **2006**, *325* (1), 170−177.
(16) Chmeliov, J.; Narkeliunas, J.; Graham, M. W.; Fleming, G. R.; Valkunas, L. Exciton−Exciton Annihilation and Relaxation Pathways in Semiconducting Carbon Nanotubes. *Nanoscale* **2016**, *8* (3), 1618−1626.
(17) Torney, D. C.; McConnell, H. M. Diffusion-Limited Reactions in One Dimension. *J. Phys. Chem.* **1983**, *87* (11), 1941−1951.
(18) Bressan, G.; Jirasek, M.; Anderson, H. L.; Heisler, I. A.; Meech, S. R. Exciton−Exciton Annihilation as a Probe of Exciton Diffusion in Large Porphyrin Nanorings. *J. Phys. Chem. C* **2020**, *124* (34), 18416−18425.
(19) Mukamel, S. *Principles of Nonlinear Optical Spectroscopy*; Oxford University Press, 1995.
(20) Malý, P.; Lüttig, J.; Rose, P. A.; Turkin, A.; Lambert, C.; Krich, J. J.; Brixner, T. Separating Single- from Multi-Particle Dynamics in Nonlinear Spectroscopy. *Nature* **2023**, *616* (7956), 280−287.
(21) Lüttig, J.; Malý, P. A. Simple Method to Extract Nonlinear Signals in Time-Resolved Spectroscopy. *J. Phys. B At. Mol. Opt. Phys.* **2026**, *59* (6), 063001.
(22) Lüttig, J.; Mueller, S.; Malý, P.; Krich, J. J.; Brixner, T. Higher-Order Multidimensional and Pump−Probe Spectroscopies. *J. Phys. Chem. Lett.* **2023**, *14* (33), 7556−7573.
(23) Bressan, G.; Peeks, M. D.; Anderson, H. L.; Meech, S. R.; Heisler, I. A. Time-Resolved Structural Dynamics of Extended π-Electron Porphyrin Nanoring. *J. Phys. Chem. C* **2019**, *123* (44), 27222−27229.
(24) Bressan, G.; Jirasek, M.; Roy, P.; Anderson, H. L.; Meech, S. R.; Heisler, I. A. Population and Coherence Dynamics in Large Conjugated Porphyrin Nanorings. *Chem. Sci.* **2022**, *13* (33), 9624−9636.
(25) Sprafke, J. K.; Kondratuk, D. V.; Wykes, M.; Thompson, A. L.; Hoffmann, M.; Drevinskas, R.; Chen, W.-H.; Yong, C. K.; Kärnbratt, J.; Bullock, J. E.; Malfois, M.; Wasielewski, M. R.; Albinsson, B.; Herz, L. M.; Zigmantas, D.; Beljonne, D.; Anderson, H. L. Belt-Shaped π-Systems: Relating Geometry to Electronic Structure in a Six-Porphyrin Nanoring. *J. Am. Chem. Soc.* **2011**, *133* (43), 17262−17273.
(26) Parkinson, P.; Kondratuk, D. V.; Menelaou, C.; Gong, J. Q.; Anderson, H. L.; Herz, L. M. Chromophores in Molecular Nanorings: When Is a Ring a Ring? *J. Phys. Chem. Lett.* **2014**, *5* (24), 4356−4361.
(27) Shi, Y.; Roy, P. P.; Higashitarumizu, N.; Lee, T.-Y.; Li, Q.; Javey, A.; Landfester, K.; McCulloch, I.; Fleming, G. R. Annihilation-Limited Long-Range Exciton Transport in High-Mobility Conjugated Copolymer Films. *Proc. Natl. Acad. Sci. U. S. A.* **2025**, *122* (17), No. e2413850122.
(28) van Stokkum, I. H. M.; Weißenborn, J.; Weigand, S.; Snellenburg, J. J. Pyglotaran: A Lego-like Python Framework for Global and Target Analysis of Time-Resolved Spectra. *Photochem. Photobiol. Sci.* **2023**, *22* (10), 2413−2431.
(29) Camargo, F. V. A.; Hall, C. R.; Anderson, H. L.; Meech, S. R.; Heisler, I. A. Time Resolved Structural Dynamics of Butadiyne-Linked Porphyrin Dimers. *Struct. Dyn.* **2016**, *3* (2), 023608.
(30) Kovalenko, S. A.; Schanz, R.; Hennig, H.; Ernsting, N. P. Cooling Dynamics of an Optically Excited Molecular Probe in Solution from Femtosecond Broadband Transient Absorption Spectroscopy. *J. Chem. Phys.* **2001**, *115* (7), 3256−3273.
(31) Rose, P. A.; Krich, J. J. Interpretations of High-Order Transient Absorption Spectroscopies. *J. Phys. Chem. Lett.* **2023**, *14* (48), 10849−10855.
(32) Krich, J. J.; Brenneis, L.; Rose, P. A.; Mayershofer, K.; Büttner, S.; Lüttig, J.; Malý, P.; Brixner, T. Separating Orders of Response in Transient Absorption and Coherent Multidimensional Spectroscopy by Intensity Variation. *J. Phys. Chem. Lett.* **2025**, *16*, 5897−5905.
(33) Völker, S. F.; Schmiedel, A.; Holzapfel, M.; Renziehausen, K.; Engel, V.; Lambert, C. Singlet−Singlet Exciton Annihilation in an Exciton-Coupled Squaraine-Squaraine Copolymer: A Model toward Hetero-J-Aggregates. *J. Phys. Chem. C* **2014**, *118* (31), 17467−17482.
(34) Bruschi, M.; Malý, P. Multi-Exciton Processes in Ultrafast Nonlinear Optical Spectroscopy. *Adv. Phys. X* **2026**, *11* (1), 2619189.
(35) Barzykin, A. V.; Tachiya, M. Stochastic Models of Charge Carrier Dynamics in Semiconducting Nanosystems. *J. Phys.: Condens. Matter* **2007**, *19* (6), 065105.
(36) Rueda Espinosa, K. J.; Kananenka, A. A. Photoexcited Energy Relaxation in Porphyrin Nanorings. *J. Phys. Chem. C* **2024**, *128* (34), 14347−14356.
(37) Spano, F. C.; Mukamel, S. Excitons in Confined Geometries: Size Scaling of Nonlinear Susceptibilities. *J. Chem. Phys.* **1991**, *95* (10), 7526−7540.
(38) Malý, P.; Lüttig, J.; Turkin, A.; Dostál, J.; Lambert, C.; Brixner, T. From Wavelike to Sub-Diffusive Motion: Exciton Dynamics and Interaction in Squaraine Copolymers of Varying Length. *Chem. Sci.* **2020**, *11* (2), 456−466.
(39) Malyshev, V. A.; Glaeske, H.; Feller, K.-H. Exciton−Exciton Annihilation in Linear Molecular Aggregates at Low Temperature. *Chem. Phys. Lett.* **1999**, *305* (1), 117−122.
(40) Tempelaar, R.; Jansen, T. L. C.; Knoester, J. Exciton−Exciton Annihilation Is Coherently Suppressed in H-Aggregates, but Not in J-Aggregates. *J. Phys. Chem. Lett.* **2017**, *8* (24), 6113−6117.
(41) Kumar, S.; Dunn, I. S.; Deng, S.; Zhu, T.; Zhao, Q.; Williams, O. F.; Tempelaar, R.; Huang, L. Exciton Annihilation in Molecular Aggregates Suppressed through Quantum Interference. *Nat. Chem.* **2023**, *15* (8), 1118−1126.
(42) Pruchyathamkorn, J.; Kendrick, W. J.; Frawley, A. T.; Mattioni, A.; Caycedo-Soler, F.; Huelga, S. F.; Plenio, M. B.; Anderson, H. L. A Complex Comprising a Cyanine Dye Rotaxane and a Porphyrin Nanoring as a Model Light-Harvesting System. *Angew. Chem., Int. Ed.* **2020**, *59* (38), 16455−16458.
(43) Yong, C.-K.; Parkinson, P.; Kondratuk, D. V.; Chen, W.-H.; Stannard, A.; Summerfield, A.; Sprafke, J. K.; O'Sullivan, M. C.; Beton, P. H.; Anderson, H. L.; Herz, L. M. Ultrafast Delocalization of Excitation in Synthetic Light-Harvesting Nanorings. *Chem. Sci.* **2015**, *6* (1), 181−189.
(44) Rouxel, R.; Lüttig, J.; Jones, M. R.; Zigmantas, D. Charting Light Harvesting in Purple Bacteria in Vivo. *Proc. Natl. Acad. Sci. U. S. A.* **2026**, *123* (27), No. e2537487123.
(45) Zhang, K.; Lee, T.-Y.; Yang, S.-J.; Bhagde, T.; Iwai, M.; Fleming, G. R. Probing Exciton Diffusion Dynamics in Photosynthetic Supercomplexes via Exciton−Exciton Annihilation. *J. Chem. Phys.* **2025**, *162* (16), 164201.
(46) Trinkunas, G.; Herek, J. L.; Polívka, T.; Sundström, V.; Pullerits, T. Exciton Delocalization Probed by Excitation Annihilation in the Light-Harvesting Antenna LH2. *Phys. Rev. Lett.* **2001**, *86* (18), 4167−4170.
(47) Hall, C. R.; Conyard, J.; Heisler, I. A.; Jones, G.; Frost, J.; Browne, W. R.; Feringa, B. L.; Meech, S. R. Ultrafast Dynamics in Light-Driven Molecular Rotary Motors Probed by Femtosecond Stimulated Raman Spectroscopy. *J. Am. Chem. Soc.* **2017**, *139* (21), 7408−7414.
(48) Bressan, G.; Heisler, I. A.; Greetham, G. M.; Edmeades, A.; Meech, S. R. Half-Broadband Two-Dimensional Electronic Spectros-

Downloaded from pubs.acs.org/jpclcd/article-pdf/doi/10.1021/acs.jpclett.6c02850/6911555l/acs.jpclett.6c02850.pdf by UNIV OF EAST ANGLIA user on 18 November 2026

https://doi.org/10.1021/acs.jpclett.6c02850
J. Phys. Chem. Lett. XXXX, XXX, XXX−XXX

copy with Active Noise Reduction. *Opt. Express* **2023**, *31* (25), 42687−42700.
(49) Harris, C. R.; Millman, K. J.; van der Walt, S. J.; Gommers, R.; Virtanen, P.; Cournapeau, D.; Wieser, E.; Taylor, J.; Berg, S.; Smith, N. J.; Kern, R.; Picus, M.; Hoyer, S.; van Kerkwijk, M. H.; Brett, M.; Haldane, A.; del Río, J. F.; Wiebe, M.; Peterson, P.; Gérard-Marchant, P.; Sheppard, K.; Reddy, T.; Weckesser, W.; Abbasi, H.; Gohlke, C.; Oliphant, T. E. Array Programming with NumPy. *Nature* **2020**, *585* (7825), 357−362.
(50) Virtanen, P.; Gommers, R.; Oliphant, T. E.; Haberland, M.; Reddy, T.; Cournapeau, D.; Burovski, E.; Peterson, P.; Weckesser, W.; Bright, J.; van der Walt, S. J.; Brett, M.; Wilson, J.; Millman, K. J.; Mayorov, N.; Nelson, A. R. J.; Jones, E.; Kern, R.; Larson, E.; Carey, C. J.; Polat, İ.; Feng, Y.; Moore, E. W.; VanderPlas, J.; Laxalde, D.; Perktold, J.; Cimrman, R.; Henriksen, I.; Quintero, E. A.; Harris, C. R.; Archibald, A. M.; Ribeiro, A. H.; Pedregosa, F.; van Mulbregt, P.; et al. SciPy 1.0: Fundamental Algorithms for Scientific Computing in Python. *Nat. Methods* **2020**, *17* (3), 261−272.

Downloaded from pubs.acs.org/jpclcd/article-pdf/doi/10.1021/acs.jpclett.6c02850/6911555l/acs.jpclett.6c02850.pdf by UNIV OF EAST ANGLIA user on 18 November 2026

https://doi.org/10.1021/acs.jpclett.6c02850
J. Phys. Chem. Lett. XXXX, XXX, XXX−XXX